Research Article

Xiaoyang Zhou, Jianlin Luo*, Jigang Zhang, Xiaoping Wu, Xuejun Tao, and Min Zhu

Fabrication of self-assembly CNT flexible film and its piezoresistive sensing behaviors

https://doi.org/10.1515/ntrev-2022-0121 received December 31, 2021; accepted May 6, 2022

Abstract: Strain sensors are essential for health monitoring of complex-shaped structures. Here, carbon nanotube thin films (CNTFS) with different double-layers were fabricated on a flexible polyethylene terephthalate substrate using layer-by-layer self-assembly technique, and their resistance behaviors and piezoresistive sensing performances were comprehensively conducted. Results show that the assembled layers of CNTFS are evenly and compactly deposited with about 7-15 µm, and the resistance decreases with the increase in the assembly layer number. The piezoresistive sensing behavior increases first and then decreases with the increase in the number of assembly layers along with compression or tension cyclic loading; the nine-double-layer CNTFS shows the best linearity, sensitivity, hysterics, and repeatability of 3.22%, 0.12684/mm, 2.16%, and 3.06%, respectively.

Keywords: structural health monitoring, carbon nanotube, flexible film, layer-by-layer self-assembly method, piezoresistive sensing performance

Xiaoyang Zhou, Xiaoping Wu, Xuejun Tao: School of Civil Engineering, Qingdao University of Technology, Qingdao 266520, China

Jigang Zhang: School of Civil Engineering, Qingdao University of Technology, Qingdao 266520, China; Collaborative Innovation Center of Engineering Construction and Safety in Shandong Blue Economic Zone, Qingdao 266033, China

Min Zhu: The Fourth Construction Co., Ltd, China Construction Eighth Engineering Division, Qingdao 266100, China

1 Introduction

Structural health monitoring (SHM) is an effective means of non-destructive monitoring of the health of structures, as defined by Housner et al., to evaluate the internal damage and servicing status of the structure, to improve structural disaster prevention and mitigation and to guide the repair and maintenance of structures [1]. Sensors are the key elements to achieving SHM. There are various embedded sensor devices used for engineering, such as resistance strain gauges (wires), piezoelectric ceramics, fatigue life wires, shape memory alloys, and fiber optic gratings [2-5], and the embedded process is generally complex, with high cost, short life, poor interference resistance and corrosion resistance, the low survival rate, and poor compatibility with concrete further weakening the structure integrity [6-8]. With the development of functional materials, piezoresistive materials, piezoelectric ceramics, and other conductive/piezoelectric materials are mixed into cement concrete matrix to make intrinsic sensing blocks, but the preparation of sensing blocks requires complex operations such as mixing, pressing, and polarization and is not suitable for practical construction [9-12]. Zhang et al. studied the mechanical, electrical, and piezoresistive properties of the electrostatic self-assembled carbon nanotube/nano carbon black (CNT/NCB) cement-based sensor. It was shown that the higher content of filler led to a significant reduction in mobility and compressive strength, whereas at lower filler content, cement hydration severely affected the resistivity of the composite, and the piezoresistive sensitivity was negatively correlated with loading rate, resulting in loss of sensing information [13-17].

Compared to the intrinsically sensitive blocks mentioned above, the flexible strain sensor can be prepared in advance, eliminating the need for onsite fabrication, and can be adapting well to the requirements of various special sizes and shapes of structures, with minimal impact on the performance of the building material itself, and with high sensitivity. Among several common strain thin-film sensors (*e.g.*, piezoresistive, piezoelectric, and capacitive-type) [18–20],

^{*} Corresponding author: Jianlin Luo, School of Civil Engineering, Qingdao University of Technology, Qingdao 266520, China; Collaborative Innovation Center of Engineering Construction and Safety in Shandong Blue Economic Zone, Qingdao 266033, China, e-mail: awjanelim@qut.edu.cn, lawjanelim2009hit@gmail.com, tel: +86 532 8507 1605, fax: +86 532 8507 1605

the piezoresistive strain gauge thin-film sensor has the advantages of easy to fabricate, no polarization required, high accuracy, and good linearity, and is well suitable to the common needs of SHM.

With the continuous development of functional materials, more and more novel piezoresistive materials have emerged, such as metal nanomaterials, conductive polymers, and carbon-based conductive materials [21-24]. Since Iijima's accidental discovery of CNTs by vacuum arc evaporation of graphite electrodes in 1991 [25,26], research around CNT has continued due to their unique mechanical [27,28], electrical [29], thermal [30,31], dielectric [32], and electromagnetic properties [33,34]. CNT has an excellent modulus of elasticity, with Young's modulus of elasticity (0.27-0.95 TPa) reported for individual multiwall CNT (MWNT) by Yu et al. [35], and for single-wall CNT (SWNT), the value is higher at 0.32-1.47 TPa [36]. This results in structural changes between the carbon elements of CNT when subjected to external forces, impeded electron movement, and changes in carrier mobility, which in turn affects macroscopic resistivity and exhibits excellent piezoresistive properties.

The piezoresistive effect of CNT-based composite is the key to their application in the field of sensors. CNT prepared by conventional methods is in the form of ultrafine powders, which can lead to agglomeration and uneven distribution during application due to side effects, high surface energy, and strong van der Waals forces between them, resulting in the material's excellent properties not being effectively exploited. Young's modulus of flexible piezoresistive nanocomposites made from a certain amount of MWNT dispersed in polydimethylsiloxane (PDMS) was investigated by Pardis et al. The results show that at a small amount of MWNT ($w_f = 0.25\%$), the inclusion of MWNT in the PDMS matrix resulted in a significant increase in Young's modulus of the nanocomposites; however, exceeding content of this nanofiller did not increase Young's modulus due to the agglomeration of MWNT inside the nanocomposite [37]. Therefore, nanomaterials should be made into macroscopic filaments, membranes, or blocks to enlarge the internal reaction surface and expand the range of molecular transfer [38], improving the mechanical and electrical properties of the nanomaterials without affecting the original properties [39–41]. There are various methods for the preparation of CNT macrobodies, such as solution spinning [42,43], array spinning [44–46], chemical vapor deposition [47], coating [48], layer-by-layer self-assembly (LBL) [49], electrophoretic deposition [50], Langmuir-Blodgett method [51,52], and blown bubble method [53]. The LBL does not require complex and expensive equipment, is used to obtain uniform

and complete films at room temperature, simple to operate, does not require an excessive investment of resources, can be in-scale produced [54], and can finely control the composition and structure by adjusting the assembly conditions (e.g., salt concentration, pH, and dipping times [55]) and the components incorporated into the film [56]. It has become the simplest and most practical of the many CNT film preparation methods. Olek et al. reported a method for the assembly of homogeneous polyelectrolyte/MWNT films on glass substrates by the LBL technique, showing that homogeneous CNT films could be produced by this method and that the structural components of the assembled layers showed strong adhesion to each other [57]. Mamedov et al. assembled uniform polyelectrolyte/MWNT films on glass substrates using the LBL technique. MWNT uniformly covered the entire surface of the glass substrate and the resulting poly(acrylic acid) (PAA)/MWNT films exhibited extremely high mechanical strength with an ultimate tensile strength of 220 ± 40 MPa, and the LBL film strength could meet the requirements of the sensor [58].

Yang et al. assembled seven layers of Pt-CNT-CHIT (polyelectrolyte chitosan)/polystyrene sulfonate films on gold substrates, placed them in a 7% phosphate solution, and stirred for 30 min, with no significant change in peak current in cyclic voltammograms (CV). The relative standard deviation of the assembled films in ten consecutive CV tests was 4.5%. This indicates that the LBL film has sufficient stability against ionic attacks [59]. The stability of LBL films was also confirmed by Hong et al. through bending tests, where 25 layers of MWNT/reduced graphene oxide (rGO) films on a polyethylene terephthalate (PET) substrate maintained their initial resistivity values after 100 times 90° bends [60]. The relationship between the number of assembled layers and the electrical properties of the films was investigated by Park et al. using the LBL method where 2-20 layers of SWNT and poly diallyl dimethylammonium chloride (PDDA) were deposited alternately on a fused silica substrate. The electrical conductivity increased continuously with the increase in the number of assembled layers, while the change in conductivity was no longer significant when the number of assembled layers exceeded 9 [61]. Zhu et al. assembled a resistive vapor-sensing device using the LBL technique, which showed excellent sensitivity, linearity, and durability in humidity-sensing tests [62].

Most LBL CNT films are prepared on rigid substrates such as silicon, glass, and metal, making them difficult to use in flexible strain gauge thin-film sensors. Ma *et al.* investigated the piezoresistive sensing characteristics of LBL MWNT/rGO-polyurethane sponges under different pressures, showing that the rate of change of resistance

gradually increased with increasing pressure and that the strain showed the same relationship with the rate of change of resistance [63]. Zhang and his team prepared LBL MWNT/PDDA human body thin films based on PDMS with tensile properties and low modulus of elasticity. It was found that the sensitivity of the LBL sensor depends on the number of layers of the MWNT assembly. By adjusting the number of layers of the assembly, sensors with different sensitivity requirements can be obtained. However, they used the two-electrode method to directly measure the resistance of the sensor through a multimeter, which could not avoid the influence of the contact resistance between the sensor film and the electrode. On the other hand, the influence of the number of LBL layers assembled on other sensor characteristics was not thoroughly studied [64–66].

In this article, a flexible CNT strain transducer was prepared based on the LBL technique. Positively charged PDDA and negatively charged carboxylated CNT were alternately deposited on a PET sheet to investigate the effect of the number of assembled layers on the resistance behaviors of the strain transducer as well as the piezoresistive sensing performance such as sensitivity, linearity, hysteresis, and repeatability.

2 Materials and test methods

2.1 Raw materials

The MWNT used in this experiment was >90% in purity, 10–20 nm in diameter, and 2–15 µm in average length.

MWNT was treated with a 3:1 volume ratio of mixed concentrated sulfuric acid and concentrated nitric acid, and the mixture was diluted by cooling in a water bath at 80° C for 4 h. After cooling, the mixture was vacuum filtered through a 0.22 μ m mixed fiber membrane and diluted several times until it reached a neutral filtrate; the mixture was dried at 50°C for 4 h to obtain carboxylated MWNT. The carboxylated MWNT dispersion was prepared at a concentration of 0.5 mg/mL and sonicated for 1 h.

PDDA was purchased from Aldrich, a 20% aqueous solution, prepared at a concentration of 15 mg/mL, with the addition of 0.5 mol/L of NaCl. NaCl increases the conductivity of the solution, increases the ionic strength, increases the ionic adsorption capacity, and helps to improve the self-assembly efficiency [67,68].

PET was selected as the assembly base, which had weak polarity, low surface energy, and weak adsorption capacity at room temperature. Therefore, the surface of PET was oxidized by ozone, and the macromolecular structure on the surface of PET was broken and wound, and the molecular chain structure and side groups were changed, forming –COOH/COOR group. The surface of PET became rough, and the adsorption capacity was enhanced [69].

2.2 Film fabrication

As shown in Figure 1, at room temperature, PET treated with ozone had a negative charge on its surface and is immersed in PDDA solution. The positively charged

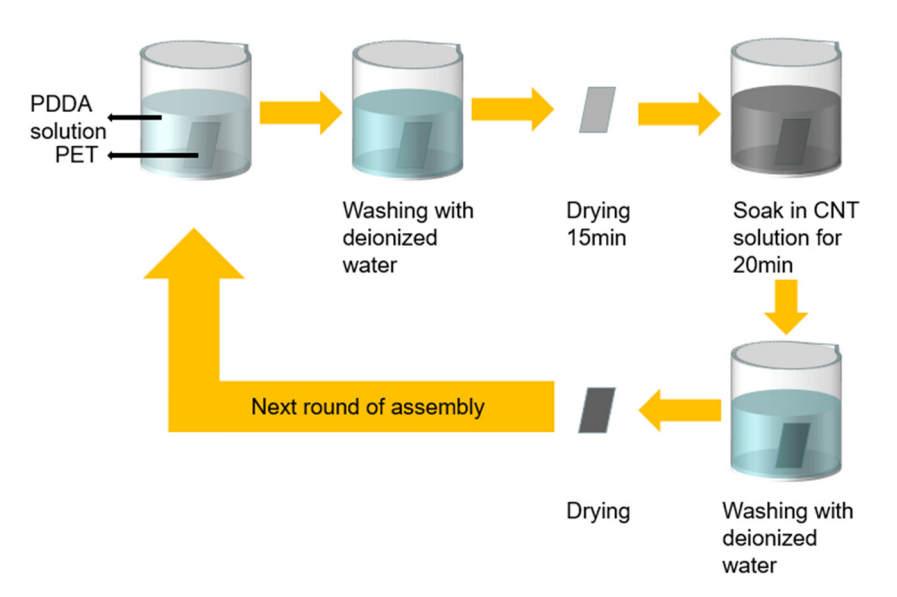


Figure 1: Assembly flowchart of self-assembly CNT film.

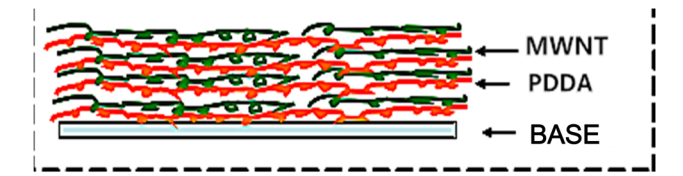


Figure 2: Schematic section structure of CNTFS.

PDDA was adsorbed on PET, and the excess PDDA was removed with deionizing water. After drying in the air for 15 min, it was immersed in CNT solution for 20 min, washed, dried to complete the first layer assembly, and repeated the above steps to proceed to the next assembly round. According to the above steps, we assembled carbon nanotube thin films (CNTFS) with 3, 6, 9, and 12 different double layers. Figure 2 shows the composition of the assembled CNTFS structure.

2.3 Test methods

The four-electrode method is used to test the resistance change of different layers of CNTFS. CNTFS, DC power supply, and standard resistance box were in-series connected, by measuring the voltage at both ends of the CNTFS and standard resistance to obtain the resistance value of CNTFS. The four-electrode method effectively avoids the contact resistance between the electrode and CNTFS caused by the electrode acting as both voltage

electrode and current electrode in the two-electrode method, which brings out more accurate resistances.

Scanning electron microscopy (SEM, S-5100 type) was used to observe the morphological characteristics of the strain gauge thin-film sensor, and the sample was broken up to observe the cross-sectional morphology.

A universal tensile testing machine (MTS (China) Ltd. Co.) was used to carry out the three-point bending test of the simply supported beam, as shown in Figure 3. The mid-span displacement of the film was controlled from 0 to 5 mm, and the loading rate was 2 mm/min. The resistance changes of the film with different assembly layers were studied under tensile and compressive stress states of the strain sensing film under five cyclic loads. And the sensor parameters involving piezoresistive linearity, sensitivity, repeatability, and hysteresis of the flexible film were comprehensively characterized.

3 Results and discussion

3.1 Morphology of CNTFS

Figure 4(a) shows SEM images of the surface of the CNTFS. Figure 4(b) and (c) shows the film cross-section, where the boundaries between the assembled layers are clear and the CNT is tightly connected to the PDDA, which is conducive to the connection between different

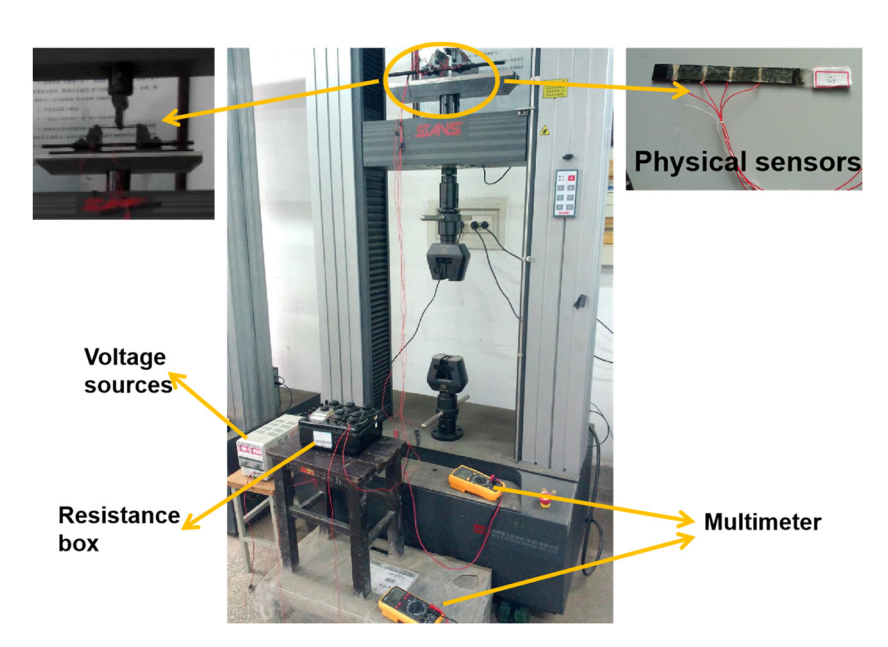


Figure 3: Piezoresistive testing of CNTFS under cyclic loading with four-electrode method by a universal testing machine.

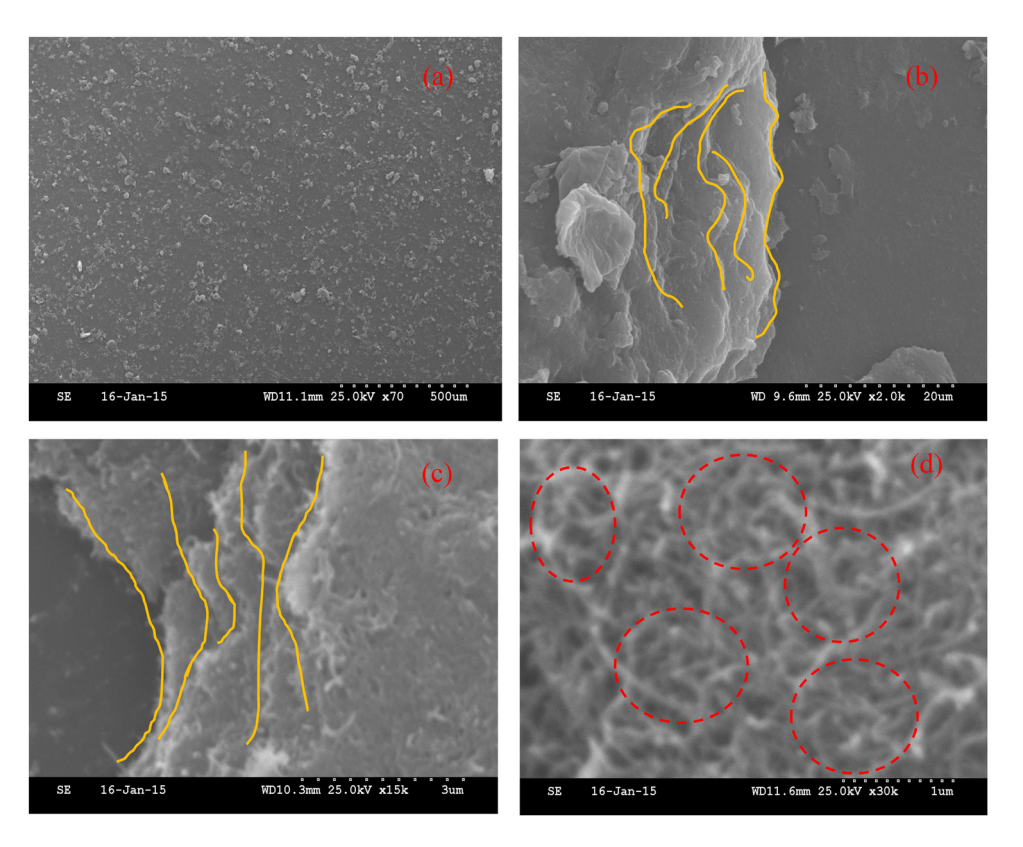


Figure 4: SEM images of self-assembled nine-double-layer CNTFS: (a) \times 70, (b) \times 2.0 k, (c) \times 15 k, and (d) \times 30 k (yellow line – assembled layer interface; dashed red circle – CNT distribution network).

layers of CNT and the improvement of electrical conductivity [70]. These pictures show that the CNT is uniformly deposited on the PET sheet, forming a dense, well-bonded, high-purity random CNT structure in the polymeric material, as shown in Figure 4(d), with a homogeneous mixture of CNT and PDDA and a stable ratio distribution, indicating a well-dispersed CNT solution.

3.2 Effect of the number of layers of CNTFS assembly on resistance properties

The trend of the film resistance properties with the number of assembled layers is shown in Figure 5. As the number of layers increases, the film resistance properties tends to decrease. It decreases rapidly at the beginning and then decreases slowly, and after the ninth layer, the trend of decreasing resistance properties is not obvious. The resistivities of 3, 6, 9, and 12 double-layer CNTFS are 127, 103, 18.3, and 7.98 k Ω cm, respectively, and the resistivity of the three-double-layer films is accordingly 15.9 times higher than that of the 12 double-layer film.

Figures 6 and 7 show that the relative rate of change in resistance is approximately linear with respect to

displacement over the displacement range of 0–5 mm. When the film is compressed, the resistance decreases ($\Delta R < 0$), and conversely when the film is stretched, the resistance increases ($\Delta R > 0$). As the number of double layers increases, the relative change in resistance is the first to show an upward trend, and the relative change in

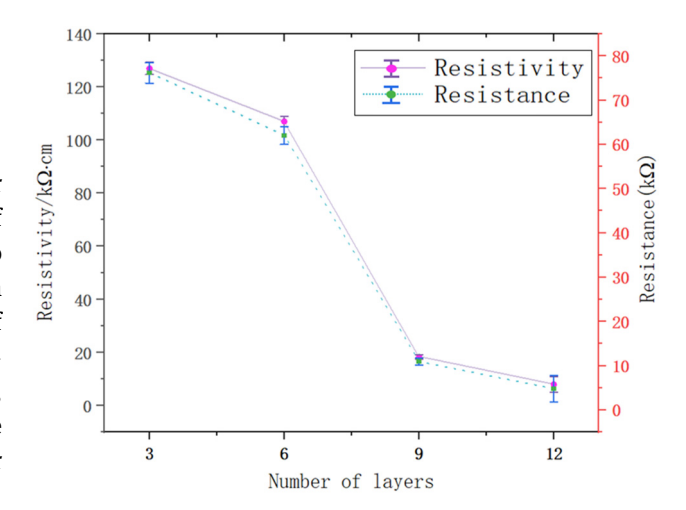


Figure 5: Relationship between the number of layers and resistance properties of CNTFS flexible film.

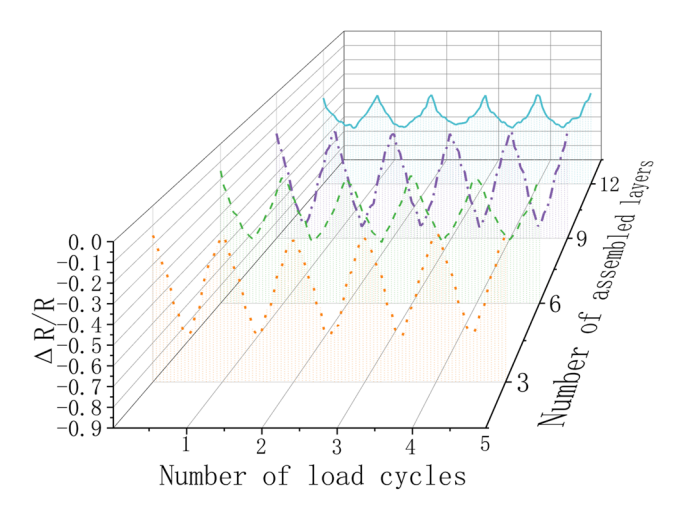


Figure 6: Relationship between change rate of resistance and midspan displacement of varied double-layer CNTFS in compression side.

resistance of the film is the largest at nine layers, reaching 80%; the relative change in resistance decreases as the number of double layers continues to increase, and the relative change in resistance of the 12-double-layer film is the smallest at about 50%.

This variation in resistance and strain can be attributed to the relationship between the change in cross-sectional area and resistance from a macroscopic point of view. We know that the resistance is inversely proportional to the cross-sectional area when all other conditions are equal. Assume that the volume of the CNTFS remains constant during compression and stretching. When the film is in compression, the cross-sectional area of the film increases and the total film resistance decreases; when the film is stretched, the cross-sectional area decreases, and the total film resistance increases in response.

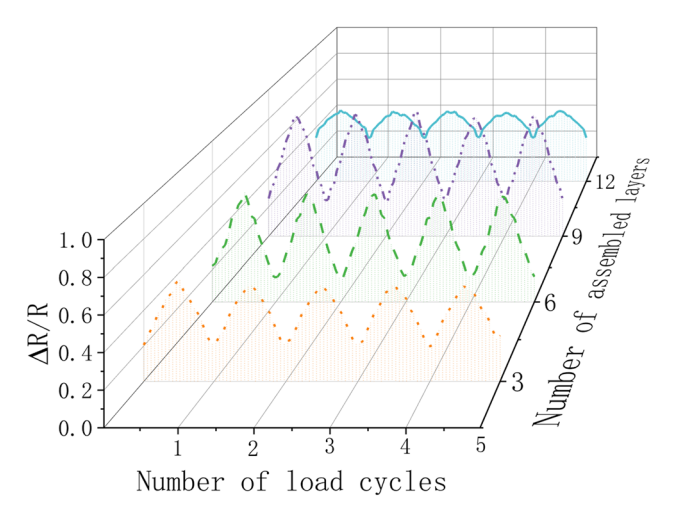


Figure 7: Relationship between change rate of resistance and midspan displacement of varied double-layer CNTFS in tension side.

From the microscopic point of view, it can be understood as the change of CNT resistance. The resistance of the CNT film consists of two parts: the CNT's own resistance (R_1) and the contact resistance (R_2) between the CNT tubes. The inter-tube contact resistance also includes the resistance R_{contact} generated by direct contact of CNT and the resistance R_{tunnel} generated by the tunneling effect. The piezoresistive effect of CNT is mainly the change in the forbidden bandwidth (E_{σ}) and the inter-tube contact resistance R_2 due to deformation [71,72]. When the film is subjected to external forces, the internal lattice structure of the CNT changes, leading to changes in the tube diameter and helix angle. causing changes in the forbidden bandwidth E_g and eventually leading to changes in the CNT's own resistance R_1 . The effect of CNT deformation on E_g was noted in the study by Jamal *et al.* The E_g of the original CNT was 0.879 eV, and the $E_{\rm g}$ of the CNT was 0.135 and 1.147 eV for 10% compression and tensile deformation, respectively [73]. Deformation also leads to changes in R_2 . Bao et al. argued that the contact between CNT and CNT occurs at the nanoscale, and the contact region consists of only a few atoms, which has a limited impact on the enhancement of conductivity [74]. Thus, film deformation mainly affects R_{tunnel} , and when the film is deformed, the tunneling chance changes subsequently, and the resistance transfer between CNTs is affected, leading to the change of R_2 . The change in film resistance is therefore the sum of the changes in R_1 and R_2 .

The influence of the tunneling effect on resistance can also explain the trend of resistance varies with the increase in assembly layers. It also confirms the interlayer connection of the CNTs in the SEM image. The PDDA only glues the CNTs to each other and does not wrap the CNTs, and the layers of CNTs are not only simply connected in parallel. When the number of assembled layers increases from 3 to 9, the CNT spacing decreases, and the tunneling probability increases. Under the condition of high CNT, the chance of direct contact between CNT is greatly increased, but CNT may appear agglomerated, which is not conducive to the formation of the conductive pathway. Moreover, mutually close, single-root CNTs that can produce tunneling effects are rarely found. It is easy to know from the circuit knowledge that when two CNTS are effectively overlapped, the current will flow through the path with low resistance formed by overlap. The formed conductive network is not easy to change under the action of external forces [75]. Therefore, when the number of assembled layers continues to increase from 9 to 12, the resistance steadily decreases (Figure 5), but the relative rate of change in resistance becomes worse (Figures 6 and 7).

Table 1: Linearity of resistivity-displacement curves for different double layers of films

Linearity	Number of load cycles	Number of double layers			
		3	6	9	12
1	Tension	3.09%	6.07%	2.58%	6.54%
	Compression	2.80%	3.33%	3.76%	3.51%
2	Tension	3.69%	3.23%	3.11%	6.31%
	Compression	4.15%	3.91%	3.99%	6.52%
3	Tension	3.74%	2.25%	2.50%	6.58%
	Compression	4.31%	3.77%	2.75%	5.89%
4	Tension	3.50%	4.46%	3.39%	6.97%
	Compression	4.26%	3.41%	3.72%	6.72%
5	Tension	3.82%	4.67%	3.11%	6.57%
	Compression	4.80%	4.40%	3.29%	6.51%
Average linearity		3.82%	<i>3.95</i> %	<i>3.22</i> %	6.21%

3.3 Effect of the number of layers of CNTFS assembly on sensing performance

The linearity δ is defined as the percentage of the maximum deviation Δ_{max} between the curve of the relative

rate of change of resistance–displacement relationship and its fitted straight line at standard conditions (20 \pm 5°C) and the full-scale output value of the relative rate of change of resistance ($\Delta R/R$)_{F,S}.

The ideal sensor should have a strict one-to-one correspondence between input and output, and the smaller the linearity value, the better. The vast majority of current flexible sensors do not have the same characteristic linearity as rigid sensors [76,77], Table 1 shows that the average linearity of the 9-double-layer film is 3.22% minimum and the average linearity of the 12-double-layer film is 6.21% maximum, with a difference of 2.89%. Yasuoka *et al.* assume that the direct contact resistance is equal to the tunneling resistance and point out that the nonlinear variation of resistance is mainly caused by the tunneling resistance [78]. It is obvious that the linearity of the 12-double-layer CNT/PDDA-PET film cannot be explained.

Figure (8b) gives the sensitivity GF of CNTFS with different assembled layers under five cycles of loading and the same variation pattern as in Table 1. Nine-double-layer films have the largest GF with the average GF value of 0.12684/mm, and 12-double-layer films have

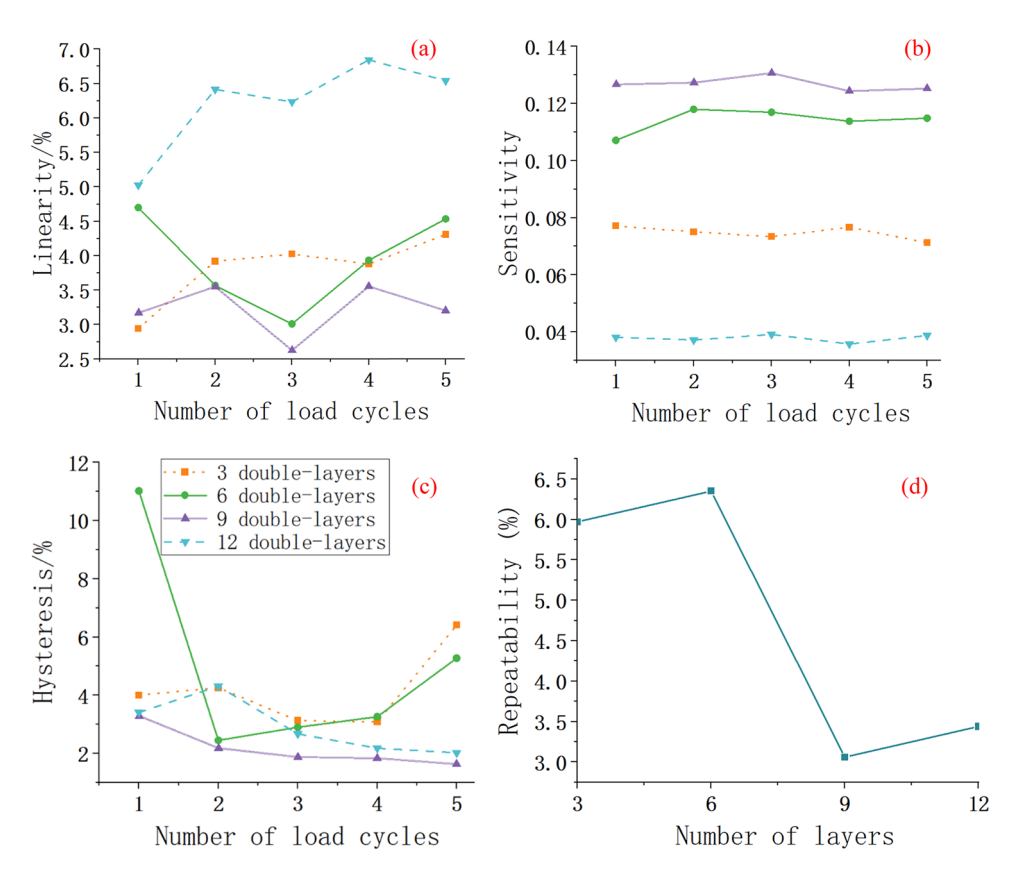


Figure 8: Effect of the number of layers of CNTFS assembly on sensing performance: (a) linearity, (b) sensitivity, (c) hysteresis, and (d) repeatability.

the smallest GF of 0.03774/mm. Nine-double-layer films have 3.36 times the GF value of 12-double-layer. Figure 8(c) shows the hysteresis curve, where hysteresis is defined as the percentage of the maximum deviation $\Delta'_{\rm max}$ between the forward and reverse travels of the resistance relative rate of change–displacement relationship curve and the full-scale output of the change rate of resistance ($\Delta R/R$)_{F.S}, which reflects the degree of non-coincidence between the forward and reverse travels of the resistance relative rate of the change–displacement curve and can be expressed as follows [79]:

$$e_z = \pm \frac{\Delta'_{\text{max}}}{(\Delta R/R)_{\text{FS}}} \times 100\%. \tag{2}$$

The smaller the hysteresis, the better the performance of the sensor. The hysteresis decreases and then increases with the increase in the number of film layers, reaching a minimum hysteresis average of 2.16% at nine layers.

Repeatability is also an important indicator to describe the sensing performance. When the displacement is changed multiple times for the full range according to the agreed direction, the degree of inconsistency in the relative rate of change of each resistance for each change–displacement, which also reflects the stability of the sensor. The repeatability error,

$$e_f = \pm \frac{1}{2} \frac{\Delta''_{\text{max}}}{(\Delta R/R)_{\text{F.S}}} \times 100\%.$$
 (3)

The e_f is described by the maximum deviation in the forward and reverse travels, as shown in Figure 8(d). The maximum repeatability error is 6.35% for the six-double-layer film, and the minimum is 3.06% for the nine-double-layer film, and the nine-double-layer CNTFS has the best sensing repeatability.

Actually, the resistance of the film decreases linearly with increasing compression displacement and increases linearly with increasing tensile displacement. Microscopically, this is because when the CNT is subjected to loading, resulting in changes in diameter and helicity, causing changes in E_g , which affects the resistance of the CNT itself. Moreover, the inter-tube distance of CNT also changes, which affects the electron transport and thus causes the inter-tube resistance of CNT to change. Macroscopic analysis suggests that under tensile displacement, the entire length of the film increases, the cross-sectional area decreases, and the overall total resistance of the film increases. In compression, the cross-sectional area decreases and the total resistance decreases.

The change rate of resistance increases with the increase in the number of assembled layers, but when the number of

assembled layers exceeds 9, the connection between CNT layers increases, and more conductive networks are formed by direct contact between CNTs, yet the chance of tunneling decreases and the change rate of resistance decreases.

4 Conclusion

- 1) The assembled layers of CNTFS are evenly and compactly deposited with about $7-15 \,\mu m$.
- 2) The resistance decreases gradually with the increase in the number of layers of film assembly, and the decreasing trend becomes flat when the number of assembled layers exceeds nine layers.
- 3) The CNTFS with varied double layers all show superior piezoresistive performance in terms of linearity, repeatability, and recoverability under five cyclic loadings. The nine-double-layer CNT film shows the most outstanding strain-sensitive performance in terms of linearity, sensitivity, hysteresis, and repeatability whose values are 3.22%, 0.12684/mm, 2.16%, and 3.06%, respectively.

Acknowledgments: The authors are obliged to the conducting mechanism discussion with Prof. Huarong Nie (Qingdao University of Science and Technology).

Funding information: This study was financially supported by the NSFC-Shandong Province Joint Key Project (Grant No. U2106222), the National Natural Science Foundation of China (No. 51878364), the project from The Fourth Construction Co., Ltd, China Construction Eighth Engineering Division, and the National "111" project, and Gaofeng discipline project funded by Shandong Province.

Author contributions: Conceptualization, supervision, and resources: Jianlin Luo, Jigang Zhang. Data curation, formal analysis, and methodology: Xiaoyang Zhou, Jianlin Luo, and Xiaoping Wu. Funding acquisition, investigation and project administration: Jianlin Luo, Jigang Zhang, and Min Zhu. Validation, visualization, and writing – original draft: Xiaoyang Zhou and Jianlin Luo. Writing – review and editing: Xiaoyang Zhou, Jianlin Luo and Xuejun Tao. All authors have accepted responsibility for the entire content of this manuscript and approved its submission.

Conflict of interest: The authors state no conflict of interest.

References

- [1] Housner GW, Bergman LA, Caughey TK, Chassiakos AG, Claus RO, Masri SF, et al. Structural control: past, present, and future. J Eng Mech. 1997;123(9):897-971.
- [2] Mohan S, Banerjee A. Modelling of minor hysteresis loop of shape memory alloy wire actuator and its application in selfsensing. Smart Mater Struct. 2021;30(5):055011.
- Tan X, Bao Y, Zhang Q, Nassif HH, Chen G. Strain transfer effect in distributed fiber optic sensors under an arbitrary field. Automat. Constr. 2021;124:103597.
- Mieloszyk M, Majewska K, Ostachowicz W. Application of embedded fibre Bragg grating sensors for structural health monitoring of complex composite structures for marine applications. Mar Struct. 2021;76:102903.
- Kosukegawa H, Berkani S, Miki H, Takagi T. Structure and electrical properties of molybdenum-containing diamond-like carbon coatings for use as fatigue sensors. Diam Relat Mater. 2017;80:38-44.
- [6] Bremer K, Wollweber M, Weigand F, Rahlves M, Kuhne M, Helbig R, et al. Fibre optic sensors for the structural health monitoring of building structures. Procedia Technol. 2016:26:524-9.
- [7] Taheri S. A review on five key sensors for monitoring of concrete structures. Constr Build Mater. 2019;204:492-509.
- [8] Su H, Zhang N, Li H. Concrete piezoceramic smart module pairs-based damage diagnosis of hydraulic structure. Compos Struct. 2018;183(Jan):582-93.
- [9] Gupta S, Gonzalez JG, Loh KJ. Self-sensing concrete enabled by nano-engineered cement-aggregate interfaces. Struct Health Monit. 2017;16(3):309-23.
- [10] Ding S, Ruan Y, Yu X, Han B, Ni YQ. Self-monitoring of smart concrete column incorporating CNT/NCB composite fillers modified cementitious sensors. Constr Build Mater. 2019;201:127-37.
- [11] Dong W, Li W, Tao Z, Wang K. Piezoresistive properties of cement-based sensors: Review and perspective. Constr Build Mater. 2019;203:146-63.
- [12] Gao S, Luo J, Zhang J, Teng F, Liu C, Feng C, et al. Preparation and piezoresistivity of carbon nanotube-coated sand reinforced cement mortar. Nanotechnol Rev. 2020;9(1):1445-55.
- [13] Zhang L, Ding S, Li L, Dong S, Wang D, Yu X, et al. Effect of characteristics of assembly unit of CNT/NCB composite fillers on properties of smart cement-based materials. Compos Part A: Appl Sci Manufac. 2018;109:303-20.
- [14] Zhang L, Han B, Ouyang J, Yu X, Sun S, Ou J. Multifunctionality of cement based composite with electrostatic self-assembled CNT/NCB composite filler. Arch Civ Mech Eng. 2017;17(2):354-64.
- [15] Han B, Zhang L, Sun S, Yu X, Dong X, Wu T, et al. Electrostatic self-assembly CNT/NCB composite fillers reinforced cementbased materials with multifunctionality. Compos. Part A: Appl Sci Manufac. 2015;79:103-15.
- [16] Zhang L, Ding S, Han B, Yu X, Ni YQ. Effect of water content on the piezoresistive property of smart cement-based materials with carbon nanotube/nanocarbon black composite filler. Compos Part A: Appl Sci Manufac. 2019;119:8-20.
- [17] Teng F, Luo J, Gao Y, Zhou X, Zhang J, Gao S, et al. Piezoresistive/piezoelectric intrinsic sensing properties of

- carbon nanotube cement-based smart composite and its electromechanical sensing mechanisms: A review. Nanotechnol Rev. 2021;10(1):1873-94.
- [18] Sarkar L, Singh SG, Vanjari SRK. Preparation and optimization of PVDF thin films for miniaturized sensor and actuator applications. Smart Mater Struct. 2021;30(7):075013.
- [19] Min SD, Wang C, Park DS, Park JH. Development of a textile capacitive proximity sensor and gait monitoring system for smart healthcare. J Med Syst. 2018;42(4):1-12.
- [20] Yoon SG, Chang ST. Microfluidic capacitive sensors with ionic liquid electrodes and CNT/PDMS nanocomposites for simultaneous sensing of pressure and temperature. J Mater Chem C. 2017;5(8):1910-9.
- [21] Singh K, Sharma S, Shriwastava S, Singla P, Gupta M, Tripathi CC. Significance of nano-materials, designs consideration and fabrication techniques on performances of strain sensors - A review. Mat Sci Semicon Proc. 2020;123(3):105581.
- [22] Jiu J, Suganuma K. Metallic nanowires and their application. IEEE T Comp Pack Man. 2016;6(12):1733-51.
- [23] Gong XX, Fei GT, Fu WB, Fang M, Gao XD, Zhong BN, et al. Flexible strain sensor with high performance based on PANI/ PDMS films. Org Electron. 2017;47:51-6.
- [24] Le TH, Kim Y, Yoon H. Electrical and electrochemical properties of conducting polymers. Polymers-basel. 2017;9(4):150.
- [25] Iijima Sumio. Helical microtubules of graphitic carbon. Nature. 1991;354(6348):56-8.
- [26] Guru K, Sharma T, Sharma T, Shukla KK, Mishra SB. Effect of Interface on the Elastic Modulus of CNT Nanocomposites. J Nanomech Micromech. 2016;6(3):04016004.
- [27] Jolowsky C, Sweat R, Park JG, Hao A, Liang R. Microstructure evolution and self-assembling of CNT networks during mechanical stretching and mechanical properties of highly aligned CNT composites. Compos Sci Technol. 2018;166:125-30.
- [28] Tsentalovich DE, Headrick RJ, Mirri F, Hao J, Behabtu N, Young CC, et al. Influence of Carbon Nanotube Characteristics on Macroscopic Fiber Properties. ACS Appl Mater Inter. 2017;9(41):36189-98.
- [29] Ebbesen TW, Lezec HJ, Hiura H, Bennett JW, Ghaemi HF, Thio T. Electrical conductivity of individual carbon nanotubes. Nature. 1996;382(6586):54-6.
- [30] Chen Y, Zhang Q, Wen X, Yin H, Liu J. A novel CNT encapsulated phase change material with enhanced thermal conductivity and photo-thermal conversion performance. Sol Energ Mat Sol C. 2018;184:82-90.
- [31] Gspann TS, Juckes SM, Niven JF, Johnson MB, Elliott JA, White MA, et al. High thermal conductivities of carbon nanotube films and micro-fibres and their dependence on morphology. Carbon. 2017;114:160-8.
- [32] Lu X, Zhang A, Dubrunfaut O, He D, Pichon L, Bai J. Numerical modeling and experimental characterization of the AC conductivity and dielectric properties of CNT/polymer nanocomposites. Compos Sci Technol. 2020;194:108150.
- [33] Wang H, Zheng K, Zhang X, Ding X, Zhang Z, Bao C, et al. 3D network porous polymeric composites with outstanding electromagnetic interference shielding. Compos Sci Technol. 2016;125:22-9.
- [34] Barathi Dassan EG, Anjang Ab Rahman A, Abidin MSZ, Akil HM. Carbon nanotube-reinforced polymer composite for

- electromagnetic interference application: A review. Nanotechnol Rev. 2020;9(1):768-88.
- [35] Yu MF, Lourie O, Dyer MJ, Moloni K, Kelly TF, Ruoff RS. Strength and breaking mechanism of multiwalled carbon nanotubes under tensile load. Science. 2000;287(5453):637-40.
- [36] Yu MF, Files BS, Arepalli S, Ruoff RS. Tensile loading of ropes of single wall carbon nanotubes and their mechanical properties. Phys Rev Lett. 2000;84(24):5552-5.
- [37] Ghahramani P, Behdinan K, Moradi-Dastjerdi R, Naguib HE. Theoretical and experimental investigation of MWCNT dispersion effect on the elastic modulus of flexible PDMS/MWCNT nanocomposites. Nanotechnol Rev. 2022;11(1):55-64.
- [38] Chen S, Luo J, Wang X, Li Q, Zhou L, Liu C, et al. Fabrication and piezoresistive/piezoelectric sensing characteristics of carbon nanotube/PVA/nano-ZnO flexible composite. Sci Rep-UK. 2020;10(1):8895.
- [39] Liu J, Hui D, Lau D. Two-dimensional nanomaterial-based polymer composites: Fundamentals and applications. Nanotechnol Rev. 2022;11(1):770–92.
- [40] Zhang L, Li L, Wang Y, Yu X, Han B. Multifunctional cementbased materials modified with electrostatic self-assembled CNT/TiO2 composite filler. Constr Build Mater. 2020;238:117787.
- [41] Zhang L, Zheng Q, Dong X, Yu X, Wang Y, Han B. Tailoring sensing properties of smart cementitious composites based on excluded volume theory and electrostatic self-assembly. Constr Build Mater. 2020;256:119452.
- [42] Mukai K, Asaka K, Wu X, Morimoto T, Okazaki T, Saito T, et al. Wet spinning of continuous polymer-free carbon-nanotube fibers with high electrical conductivity and strength. Appl Phys Express. 2016;9(5):055101.
- [43] He Z, Zhou G, Byun JH, Lee SK, Um MK, Park B, et al. Highly stretchable multi-walled carbon nanotube/thermoplastic polyurethane composite fibers for ultrasensitive, wearable strain sensors. Nanoscale. 2019;11(13):5884-90.
- [44] Qiu L, Wang X, Tang D, Zheng X, Norris PM, Wen D, et al. Functionalization and densification of inter-bundle interfaces for improvement in electrical and thermal transport of carbon nanotube fibers. Carbon. 2016;105:248–259.
- [45] Jiang Q, Wu L. Property enhancement of aligned carbon nanotube/polyimide composite by strategic prestraining. J Reinf Plast Comp. 2016;35(4):287-94.
- [46] Nam TH, Goto K, Yamaguchi Y, Premalal EVA, Shimamura Y, et al. Improving mechanical properties of high volume fraction aligned multi-walled carbon nanotube/epoxy composites by stretching and pressing. Compos. B Eng. 2016;85:15-23.
- [47] Zhang Z, Zhang Y, Jiang X, Bukhari H, Zhang Z, Han W, et al. Simple and efficient pressure sensor based on PDMS wrapped CNT arrays. Carbon. 2019;155:71–76.
- [48] Wu D, Wei M, Li R, Xiao T, Gong S, Xiao Z, et al. A percolation network model to predict the electrical property of flexible CNT/PDMS composite films fabricated by spin coating technique. Compos B Eng. 2019;174:107034.
- [49] Shajari S, Ramakrishnan S, Karan K, Sudak LJ, Sundararaj U. Ultrasensitive wearable sensor with novel hybrid structures of silver nanowires and carbon nanotubes in fluoroelastomer: Multi-directional sensing for human health monitoring and stretchable electronics. Appl Mater Tody. 2022;26:101295.

- [50] Atiq Ur Rehman M, Chen Q, Braem A, Shaffer MSP, Boccaccini AR. Electrophoretic deposition of carbon nanotubes: recent progress and remaining challenges. Int Mate Rev. 2021;66(8):533–62.
- [51] Zhang J, Wang M, Yang Z, Zhang X. Highly flexible and stretchable strain sensors based on conductive whisker carbon nanotube films. Carbon. 2021;176:139-47.
- [52] Stanković NK, Todorović-Marković BM, Marković ZM. Selfassembly of carbon based nanoparticles films by Langmuir-Blodgett method. J Serb Chem Soc. 2020;85(9):1095–127.
- [53] Wu S, Shi E, Yang Y, Xu W, Li X, Cao A. Direct fabrication of carbon nanotube-graphene hybrid films by a blown bubble method. Nano Res. 2015;8(5):1746-54.
- [54] Gupta S, Heintzman E, Price C. Electrostatic layer-by-layer self-assembled graphene/multi-walled carbon nanotubes hybrid multilayers as efficient 'all carbon'supercapacitors. J Nanosci Nanotechno. 2016;16(5):4771–82.
- [55] Tang X, Cheng D, Ran J, Li D, He C, Bi S, et al. Recent advances on the fabrication methods of nanocomposite yarn-based strain sensor. Nanotechnol Rev. 2021;10(1):221-36.
- [56] Arslan M, Dönmez G, Ergün A, Okutan M, Albayrak Arı G, Deligöz H. Preparation, characterization, and separation performances of novel surface modified LbL composite membranes from polyelectrolyte blends and MWCNT. Polym Eng Sci. 2020;60(2):341–51.
- [57] Olek M, Ostrander J, Jurga S, Möhwald H, Kotov N, Kempa K, et al. Layer-by-Layer assembled composites from Multiwall carbon nanotubes with different morphologies. Nano Lett. 2004;4(10):1889-95.
- [58] Mamedov AA, Kotov NA, Prato M, Guldi DM, Wicksted JP, Hirsch A. Molecular design of strong single-wall carbon nanotube/polyelectrolyte multilayer composites. Nat Mater. 2002;1(3):190-4.
- [59] Yang M, Yang Y, Yang H, Shen G, Yu R. Layer-by-layer selfassembled multilayer films of carbon nanotubes and platinum nanoparticles with polyelectrolyte for the fabrication of biosensors. Biomaterials. 2006;27(2):246-55.
- [60] Hong TK, Lee DW, Choi HJ, Shin HS, Kim BS. Transparent, flexible conducting hybrid multilayer thin films of multiwalled carbon nanotubes with graphene nanosheets. ACS Nano. 2010;4(7):3861–8.
- [61] Park YT, Ham AY, Grunlan JC. High electrical conductivity and transparency in deoxycholate-stabilized carbon nanotube thin films. J Phys Chem C. 2010;114(14):6325–33.
- [62] Zhu P, Kuang Y, Wei Y, Li F, Ou H, Jiang F, et al. Electrostatic self-assembly enabled flexible paper-based humidity sensor with high sensitivity and superior durability. Chem Eng J. 2021;404:127105.
- [63] Ma Z, Wei A, Ma J, Shao L, Jiang H, Dong D, et al. Lightweight, compressible and electrically conductive polyurethane sponges coated with synergistic multiwalled carbon nanotubes and graphene for piezoresistive sensors. Nanoscale. 2018;10(15):7116-26.
- [64] Zhang P, Chen Y, Li Y, Zhao Y, Wang W, Li S, et al. Flexible piezoresistive sensor with the microarray structure based on self-assembly of multi-walled carbon nanotubes. Sensors. 2019;19(22):4985.
- [65] Wang W. Human flexible strain sensor based on PDMS/ MWCNTs Layer-by-Layer Self-assembly. Thesis Shandong Univ Sci Technol. 2020 (in Chinese).

- [66] Wang W, Chen D, Liu J, Zhu J, Zhang P, Yang L, et al. Strain sensor for full-scale motion monitoring based on self-assembled PDMS/ MWCNTs layers. J Phys D Appl Phys. 2019;53(9):095405.
- [67] Zhang D, Tong J, Xia B, Xue Q. Ultrahigh performance humidity sensor based on Layer-by-layer self-assembly of graphene oxide/polyelectrolyte nanocomposite film. Sensor. Actuat B-Chem. 2014;203:263-70.
- [68] Xiang Y, Lu S. Layer-by-layer self-assembly in the development of electrochemical energy conversion and storage devices from fuel cells to supercapacitors. Chem Soc Rev. 2012;41(21):7291-321.
- [69] Khanchaitit P, Aht-Ong D. Continuous surface modification process with ultraviolet/ozone for improving interfacial adhesion of poly (ethylene terephthalate)/epoxy composites. Polym Compos. 2006;27(5):484-90.
- [70] Gao E, Cao Y, Liu Y, Xu Z. Optimizing interfacial cross-linking in graphene-derived materials, which balances intralayer and interlayer load transfer. ACS Appl Mater Inter. 2017;9(29):24830-9.
- [71] Lyapkosova OS, Lebedev NG. Piezoresistive effect in singlewalled carbon nanotubes. Phys Solid State. 2012;54(7):1501-6.
- [72] Grow RJ. Electromechanical properties and applications of carbon nanotubes. Carbon nanotubes properties and applications. USA: CRC Press; 2018. p. 187-212.

- [73] Talla JA, Alsalieby AF. Effect of uniaxial tensile strength on the electrical properties of doped carbon nanotubes: density functional theory. Chin J Phys. 2019;59:418-25.
- [74] Bao WS, Meguid SA, Zhu ZH, Weng GJ. Tunneling resistance and its effect on the electrical conductivity of carbon nanotube nanocomposites. J Appl Phys. 2012;111(9):7492.
- [75] Sun YY. Study on the Linearization of the Pressure Sensors Made of CNT/polymer Composite. Thesis Southwest Univ Sci Technol. 2019 (in Chinese).
- [76] Gao Y, Luo J, Zhang J, Zhou X, Teng F, Liu C, et al. Repairing performances of novel cement mortar modified with graphene oxide and polyacrylate polymer. Nanotechnol Rev. 2022;11(1):1778-91.
- [77] Sanli A, Kanoun O. Electrical impedance analysis of carbon nanotube/epoxy nanocomposite-based piezoresistive strain sensors under uniaxial cyclic static tensile loading. J Compos Mater. 2020;54(6):845-55.
- [78] Yasuoka T, Shimamura Y, Todoroki A. Electrical resistance change under strain of CNF/flexible-epoxy composite. Adv Compos Mater. 2010;19(2):123-38.
- [79] He Y, Ming Y, Li W, Li Y, Wu M, Song J, et al. Highly Stable and Flexible Pressure Sensors with Modified Multi-Walled Carbon Nanotube/Polymer Composites for Human Monitoring. Sensors. 2018;18(5):1338.